Laboratory Investigation (2021) 101:878–896
https://doi.org/10.1038/s41374-021-00578-6

ARTICLE

Amelioration of circadian disruption and calcium-handling protein defects by choline alleviates cardiac remodeling in abdominal aorta coarctation rats

Xi He[1] · Si Yang[1] · Juan Deng[1] · Qing Wu[1] · Wei-Jin Zang[1]

Received: 24 September 2020 / Revised: 5 February 2021 / Accepted: 5 February 2021 / Published online: 1 March 2021

Abstract

The key pathophysiological process leading to heart failure is cardiac remodeling, a term referring to cardiac hypertrophy, fibrosis, and apoptosis. We explored circadian rhythm disruption and calcium dyshomeostasis in cardiac remodeling and investigated the cardioprotective effect of choline. The experiments were conducted using a model of cardiac remodeling by abdominal aorta coarctation (AAC) in Sprague–Dawley rats. In vitro cardiomyocyte remodeling was induced by exposing neonatal rat cardiomyocytes to angiotensin II. The circadian rhythms of the transcript levels of the seven major components of the mammalian clock (*Bmal1*, *Clock*, *Rev-erbα*, *Per1/2*, and *Cry1/2*) were altered in AAC rat hearts during a normal 24 h light/dark cycle. AAC also upregulated the levels of proteins that mediate store-operated Ca^{2+} entry/receptor-operated Ca^{2+} entry (stromal interaction molecule 1 [STIM1], Orai1, and transient receptor potential canonical 6 [TRPC6]) in rat hearts. Moreover, choline ameliorated circadian rhythm disruption, reduced the upregulated protein levels of STIM1, Orai1, and TRPC6, and alleviated cardiac dysfunction and remodeling (evidenced by attenuated cardiac hypertrophy, fibrosis, and apoptosis) in AAC rats. In vitro analyses showed that choline ameliorated calcium overload, downregulated STIM1, Orai1, and TRPC6, and inhibited thapsigargin-induced store-operated Ca^{2+} entry and 1-oleoyl-2-acetyl-sn-glycerol-induced receptor-operated Ca^{2+} entry in angiotensin II-treated cardiomyocytes. In conclusion, choline attenuated AAC-induced cardiac remodeling and cardiac dysfunction, which was related to amelioration of circadian rhythm disruption and attenuation of calcium-handling protein defects. Modulation of vagal activity by choline targeting the circadian rhythm and calcium homeostasis may have therapeutic potential for cardiac remodeling and heart failure.

Introduction

Heart failure is commonly the consequence of sustained abnormal neurohormonal and mechanical stress and is a major cause of mortality in patients with cardiovascular disease worldwide. The key pathophysiological process leading to heart failure is cardiac remodeling, a term referring to cardiac hypertrophy, fibrosis, and apoptosis [1, 2]. The impaired cardiovascular functions and the elevated morbidity and mortality in heart failure are closely related to autonomic imbalance characterized by suppressed vagal (parasympathetic) activity and increased sympathetic activity. Moreover, the magnitude of sympathovagal imbalance is associated with the outcome [3, 4]. Therefore, activation of the vagal nervous system may have beneficial implications for the treatment of cardiovascular diseases and many studies have focused on the importance of elevating vagal activity [5, 6]. Studies of vagal stimulation in human heart failure were encouraging, reporting beneficial effects on functional capacity and life quality [7]. Choline, a precursor for biosynthesis of the vagal nerve neurotransmitter acetylcholine (ACh), has a remarkable protective effect against a variety of cardiovascular diseases [8, 9]. It ameliorates cardiac damage in spontaneously hypertensive rats by correcting abnormal DNA methylation and regulating 2-oxoglutarate/ten-eleven translocation methylcytosine dioxygenase enzymes [8]. In addition, it attenuates ischemia/reperfusion-induced vascular dysfunction by inhibiting Ca^{2+}/calmodulin-dependent protein kinase II [9]. However, the molecular mechanisms underlying the cardioprotective effects of choline during cardiac remodeling are not fully understood.

✉ Wei-Jin Zang
zwj@xjtu.edu.cn

[1] Department of Pharmacology, School of Basic Medical Sciences, Xi'an Jiaotong University Health Science Center, Xi'an, PR China

Circadian rhythms play important roles in cardiovascular physiology and behavior; disruption of these rhythms may lead to cardiovascular disease. The circadian rhythms generated by the molecular clocks in the suprachiasmatic nucleus and peripheral tissues are maintained by autoregulatory transcriptional and translational feedback loops involving multiple clock genes, such as brain and muscle Arnt-like protein-1 (*Bmal1*), circadian locomotor output cycles protein kaput (*Clock*), cryptochrome 1 and 2 (*Cry1* and *Cry2*) and period 1–3 (*Per1–Per3*), and their proteins, which are required for the generation of circadian rhythms [10]. In addition to the master clock which resides in the suprachiasmatic nucleus, each peripheral tissue or organ including the heart and vasculature also possesses an intrinsic circadian rhythm termed the peripheral clock. The central clock orchestrates the phase of each peripheral clock through the autonomic nervous system or humoral factors. The peripheral clock plays an important role in maintaining tissue or organ homeostasis [11]. The heart possesses a fully functional internal clock. However, few studies have investigated changes in the circadian clock of the heart in the context of AAC and heart failure. How the circadian oscillator in hearts coordinates and regulates heart physiology in response to the vagal nervous system remains unclear.

Stromal interaction molecule 1 (STIM1) and calcium-release activated calcium channels (Orai1) play important roles in hypertrophy-related contractile dysfunction [12]. STIM1 and Orai1 channels are the major components of store-operated Ca^{2+} channels (SOCC), leading to store-operated Ca^{2+} entry (SOCE) [13, 14]. SOCE is a mechanism by which Orai1 in the sarcolemma senses depletion of intracellular calcium and opens to allow an influx of extracellular calcium; this process is enhanced during pathological cardiac remodeling [15]. STIM1 functions as a sarcoplasmic reticulum Ca^{2+} sensor and plays an important role in detecting Ca^{2+} depletion and activating Orai1 channels. Depletion of STIM1 prevented cardiac hypertrophy in rats [16], while overexpression of STIM1 in adult rat cardiomyocytes resulted in aberrant Ca^{2+} handling and cardiomyopathy [17]. Receptor-operated Ca^{2+} channels (ROCC) are activated by ligand binding to membrane receptors. The transient receptor potential canonical (TRPC) channels, such as TRPC6, are the major components of ROCC responsible for receptor-operated Ca^{2+} entry (ROCE) [14]. Ca^{2+} signaling plays an essential role in a wide range of cellular functions, which underscores the importance of understanding the mechanisms involved in regulating Ca^{2+} homeostasis in cardiomyocytes under both physiological and pathophysiological conditions. The effects of choline on circadian rhythms and SOCC/ROCC-mediated calcium influx in pathological cardiac remodeling have not been characterized. In this study, experiments were conducted using a classic model of cardiac remodeling by abdominal aorta coarctation (AAC) in Sprague–Dawley rats. Angiotensin II (Ang II) is a primary effector peptide of the renin-angiotensin system (RAS) and directly promotes cardiac cell death, hypertrophy, and remodeling. In vitro cardiomyocyte remodeling was induced by exposing neonatal rat cardiomyocytes to Ang II. We investigated whether choline may ameliorate AAC or Ang II-induced cardiomyocyte remodeling by alleviating circadian rhythm disruption and calcium dyshomeostasis.

Materials and methods

Animals and manipulations

Adult male Sprague–Dawley rats (8 weeks old) were purchased from the Experimental Animal Centre of Xi'an Jiaotong University. This study was conducted in strict accordance with the Guidelines for the Care and Use of Laboratory Animals (National Institutes of Health publication, eighth edition, 2011). All experimental procedures were approved by the Ethics Committee of Xi'an Jiaotong University. Rats were anesthetized with sodium pentobarbital (45 mg/kg, intraperitoneally), and cardiac remodeling was induced by coarctation of the abdominal aorta, as described previously [18]. The diameter of the lumen of the aorta after coarctation was equivalent to that of a 22-gauge needle (0.7 mm). In sham animals, sham operations were performed without coarctation of the aorta. Seven days after aortic coarctation, the rats were randomly divided into four experimental groups; namely, the sham, sham + choline, AAC, and AAC + choline groups. The rats were administered choline (Sigma, St. Louis, MO, USA) at 7 mg/kg per day or vehicle by intraperitoneal injection once per day for 12 weeks (Fig. 1a). Rats were housed in an environment-controlled room, in which a strict 12 h light/12 h dark cycle was enforced (lights on at 7 AM; zeitgeber time [ZT] 0). On the day of the experiment, rats were euthanized at 6 h intervals from 7 AM to 7 AM the following day. To ensure the reproducibility of the gene expression cycles, one animal per group was euthanized at each time point on three separate days. All rats were anesthetized with sodium pentobarbital (45 mg/kg, intraperitoneally). The right carotid artery was exposed and cannulated with a catheter that was connected to the pressure transducer for recording blood pressure. At the end of the study, the rats were euthanized with sodium pentobarbital (100 mg/kg, intraperitoneally).

Echocardiography

For transthoracic echocardiography, rats were anesthetized with 1.5–2% inhalational isoflurane, placed on a heating pad and imaged using the Vevo 2100 High Resolution Imaging System (Visual Sonics Inc., Toronto, ON, Canada).

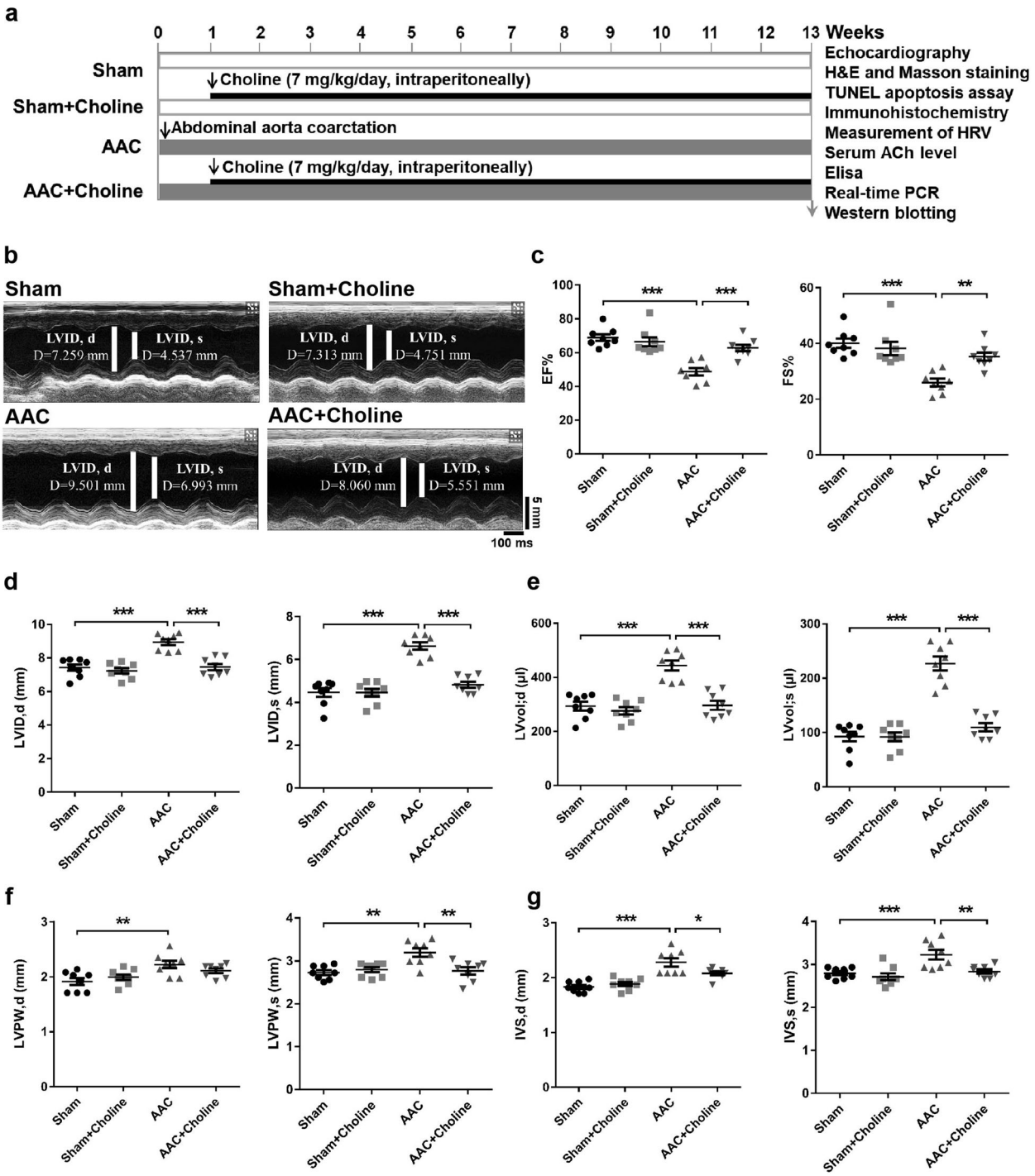

Fig. 1 Effect of choline on cardiac function in an abdominal aortic coarctation (AAC) rat model. a Experimental protocol. **b** Representative echocardiographic images of rat hearts. **c** EF ejection fraction, FS fractional shortening. **d** LVID, d, left ventricle internal dimension in diastole; LVID, s, left ventricle internal dimension in systole. **e** LVvol; d, left ventricle end-diastolic volume; LVvol; s, left ventricle end-systolic volume. **f** LVPW, d, thickness of left ventricle posterior wall in diastole; LVPW, s, thickness of left ventricle posterior wall in systole. **g** IVS, d, thickness of the interventricular septum in diastole; IVS, s, thickness of the interventricular septum in systole. Data are means ± SEM ($n = 8$ rats per group). $^{*}P < 0.05$, $^{**}P < 0.01$, $^{***}P < 0.001$.

Echocardiographic parameters included the left ventricle ejection fraction (EF), left ventricle fractional shortening (FS), left ventricle internal dimension in diastole (LVID, d) and systole (LVID, s), left ventricle end-diastolic volume (LVvol; d), left ventricle end-systolic volume (LVvol; s), thickness of the left ventricle posterior wall in diastole (LVPW, d) and systole (LVPW, s), and thickness of the interventricular septum in diastole (IVS, d) and systole (IVS, s).

Histological analysis of heart tissues

Rat heart tissues were fixed in 4% paraformaldehyde, dehydrated, embedded in paraffin and cut into 4 μm-thick sections. Sections were dewaxed with xylene, rehydrated with decreasing grades of ethanol, and rinsed with distilled water. Next, the heart sections were stained with hematoxylin and eosin and Masson's trichrome. The cardiomyocyte cross-sectional diameter, cardiomyocyte area, and cardiac fibrosis area were analyzed using ImageJ software (National Institutes of Health, Bethesda, MD, USA). Terminal deoxynucleotidyl transferase-mediated dUTP nick-end labelling (TUNEL) staining was performed using a TUNEL Apoptosis Assay Kit (Wanleibio, Shenyang, China) according to the manufacturer's instructions. Briefly, the heart sections were rinsed with 50 μl TUNEL reaction mixture for 90 min at 37 °C in the dark. The sections were developed with 3,3′-diaminobenzidine and counterstained with hematoxylin, and then mounted in neutral balsam mounting medium. Images were captured using a light microscope (Eclipse Ci-L, Nikon Instruments Inc., Tokyo, Japan).

Immunohistochemistry

Standard immunohistochemical staining protocols were performed as described previously [19]. Heart tissue sections of 4 μm thickness were blocked with 10% goat serum for 30 min, and incubated with a primary antibody against atrial natriuretic peptide (ANP, 1:200; Abcam, Cambridge, UK), brain natriuretic peptide (BNP, 1:300; WanleiBio), or β-myosin heavy chain (β-MHC, 1:200; Proteintech, Wuhan, China) overnight at 4 °C. The sections were washed with phosphate-buffered saline (PBS, three times for 5 min each) and incubated at 37 °C in horseradish peroxidase-conjugated goat anti-rabbit IgG for 50 min. After washing, sections were stained with 3, 3′-diaminobenzidine and counterstained with hematoxylin. Finally, the slides were dehydrated, cleared, and mounted for light microscopy (Eclipse Ci-L, Nikon Instruments Inc., Tokyo, Japan).

Measurement of heart rate variability

Heart rate (HR) analysis and power spectrum analysis of HR variability were made on an electrocardiogram processor analyzing system. The root mean square successive difference (RMSSD) in heart period series is a time domain measure of HR variability. We used frequency bands of low frequency (LF) (0.04–0.15 Hz) and high frequency (HF) (0.15–0.40 Hz) according to a previous study [18]. The ratio of LF and HF power (LF/HF) was also calculated. The LF spectral component is a marker of sympathetic modulation, the HF component is a marker of vagal modulation, and the LF/HF ratio is a marker of sympathovagal balance.

Determination of serum levels of ACh

After rats were anesthetized, blood samples were obtained via the abdominal aortic method. Blood samples were centrifuged at 3000 *rpm* for 10 min at 4 °C and serum was aliquoted and stored at –80 °C until assay. Serum levels of ACh were measured with commercial colorimetric kit (Jiancheng Biochemical Co., Ltd., Nanjing, China) according to the manufacturer's instructions. The absorbance at 550 nm was read on a Stat Fax 2100 spectrophotometer (Awareness Technology, Palm City, FL, USA).

Enzyme linked immunosorbent assay (ELISA)

The serum level of catecholamine (CA), cardiac angiotensin converting enzyme (ACE) activity, and cardiac cyclic adenosine monophosphate (cAMP) concentration were evaluated by specific ELISAs using commercial kits (Jianglai biotech, Shanghai, China) in accordance with the manufacturer's instructions.

RNA extraction and real-time quantitative PCR

Total RNA was isolated from heart tissues using a Total RNA Kit (Omega Biotek, Norcross, GA, USA) according to the manufacturer's instructions. Equal amounts of RNA were reverse transcribed to cDNA using PrimeScript™ RT Master Mix (TaKaRa, Tokyo, Japan). Gene expression was analyzed using a Real-Time PCR system (Exicycler 96, Bioneer, Daejeon, Korea) with SYBR Premix Ex Taq (TaKaRa) and gene-specific primers. The primers were as follows: Clock, forward 5′-GCAGTGGATTTGGCTTCA-3′, and reverse 5′-AGTTCTCGCCGTCTTTCA-3′; Bmal1, forward 5′-GTGCCACCAACCCATACA-3′, and reverse 5′-TCTTCCCTCGGTCACATC-3′; Rev-erbα, forward 5′-TTAACGGCATGGTGCTACT-3′, and reverse 5′-TTGCGATTGATACGGACA-3′; Per1, forward 5′-GCGGAGTTCTCACAGTTCA-3′, and reverse 5′-CCACTGGTAGACGGGTTGT-3′; Per2, forward 5′-CTACCCAGCTACCCGTTTC-3′, and reverse 5′-GCAGGAGTTATTTCAGAGGC-3′; Cry1, forward 5′-CCGACGACCATGATGAGA-3′, and reverse 5′-CTTGCGAGCAGGGAGTTT-3′; Cry2, forward 5′-AGGACTACGGCTCCACGAC-3′, and reverse 5′-GGTTGATGCCCACTGACG-3′; β-actin, forward 5′-GGAGATTACTGCCCTGGCTCCTAGC-3′, and reverse 5′-GGCCGGACTCATCGTACTCCTGCTT-3′. The PCR reactions were initiated with denaturation at 94 °C for 5 min, followed by amplification for 40 cycles of 94 °C for 10 s, 60 °C for 20 s, and 72 °C for 30 s. All samples were analyzed in triplicate. Relative gene expression levels

were determined using the $2^{-\Delta\Delta Ct}$ method, with normalization to the internal control, β-actin.

Primary cardiomyocyte isolation and culture

Primary neonatal rat ventricular cardiomyocytes (NRVCs) were prepared as described previously [20]. Briefly, cardiac ventricles from 1-day-old neonatal Sprague–Dawley rats were separated and cut into small pieces, and then digested with 0.1% collagenase until the tissues were completely digested. Next, cells were combined, centrifuged, and resuspended in low-glucose Dulbecco's modified Eagle's medium containing 10% fetal bovine serum. The cardiomyocytes were separated from fibroblasts based on their differential adhesion. After incubation for 1 h, the non-adhered cells were cultured in low-glucose Dulbecco's modified Eagle's medium containing 10% fetal bovine serum and antibiotics (0.1 mg/ml streptomycin and 100 U/ml penicillin) in a humidified atmosphere containing 5% CO_2 at 37 °C. The culture medium was changed every 24 h. Cardiomyocyte purity was characterized by positive staining with α-actinin antibody (1:200; Thermo Fisher Scientific, Rockford, IL, USA). Where indicated, the serum-starved cells were incubated for 24 h in serum-free Dulbecco's modified Eagle's medium containing 10^{-7} M Ang II (Sigma) and/or 0.5 mM choline (Sigma). The concentrations of Ang II [21, 22] and choline [18] were selected according to previous reports.

Fluorescence imaging of intracellular Ca^{2+}

Measurement of the intracellular Ca^{2+} level was performed as described previously [14, 23]. Briefly, cultured NRVCs plated on 15 mm glass-bottom cell culture dishes were loaded with 5 μM Ca^{2+} sensitive dye Fluo-4 acetoxymethyl ester (Thermo Fisher Scientific) at 37 °C for 30 min. Next, cells were washed three times with Tyrode solution (mM: 140 NaCl, 4.7 KCl, 10 glucose, 1.2 $MgCl_2$, 1.8 $CaCl_2$, and 10 4-(2-hydroxyethyl)−1-piperazineethanesulfonic acid [pH 7.4]). Cells were monitored using a confocal laser scanning microscope (Nikon C2, Nikon, Tokyo, Japan). Fluorescence values with excitation at 488 nm and emission at 516 nm were measured consecutively. Fluo-4 images were analyzed using NIS Elements software version 3.20.02 (Nikon). F is the real-time fluorescence intensity and F_0 is the steady-state condition fluorescence value; intracellular Ca^{2+} changes are reported as the ratio F/F_0. To study SOCE, cells were incubated with Ca^{2+}-free Tyrode solution and maintained for 15 min before use to allow passive depletion of intracellular Ca^{2+} stores and de-esterification of Fluo-4 acetoxymethyl ester. In Ca^{2+}-free solution, $CaCl_2$ was replaced by equimolar $MgCl_2$, and 0.1 mM ethylene glycol-bis (β-aminoethyl ether)-N,N,N′,N′-tetraacetic acid was added to chelate residual Ca^{2+}. Cells were incubated in Ca^{2+}-containing Tyrode solution supplemented with 1 μM thapsigargin (TG). Extracellular application of the membrane-permeable diacylglycerol analogue, 1-oleoyl-2-acetyl-sn-glycerol (OAG, 100 μM; Sigma), can directly activate ROCC and induce ROCE.

Protein preparation and Western blotting

Rat heart tissues and NRVCs were lysed in radioimmunoprecipitation assay buffer (Beyotime Institute of Biotechnology, Shanghai, China) containing protease inhibitor cocktail. Cell lysate was centrifuged at 13,000 *rpm* for 10 min at 4 °C, and the supernatants were used as samples. Equal amounts of protein (30 μg) were separated in sodium dodecyl sulfate-polyacrylamide gels and transferred to polyvinylidene fluoride membranes (Immobilon P; Millipore, Billerica, MA, USA). After blocking with 5% skim milk in Tris-buffered saline supplemented with 0.1% Tween 20 for 1 h at room temperature, the membranes were incubated at 4 °C overnight with a primary antibody against β1-adrenergic receptor (β1-AR, diluted 1:1000; Abcam), α-MHC (diluted 1:2000; Proteintech), β-MHC (diluted 1:600; Proteintech), STIM1 (diluted 1:1000; Proteintech), Orai1 (diluted 1:1000; Abclonal, Cambridge, MA, USA), TRPC6 (diluted 1:1000; Proteintech), or GAPDH (diluted 1:5000; Affinity Biosciences). GAPDH was used as the internal loading control. The membranes were incubated with the appropriate horseradish peroxidase-conjugated secondary antibodies (Affinity Biosciences) at 1:5000 dilution for 40 min at room temperature. Bands were visualized with ECL-Plus reagent (Millipore), and the band density was quantified using Gel-Pro Analyzer (Media Cybernetics, Bethesda, MD, USA).

Statistical analysis

Data are expressed as means ± SEM. Differences among multiple groups were analyzed by one-way analysis of variance (ANOVA) followed by Tukey multiple-comparison *post hoc* test. All statistical analyses were performed using Prism software (version 7.0; GraphPad Inc, La Jolla, CA, USA). In all analyses, $P < 0.05$ was taken to indicate statistical significance.

Results

Choline ameliorated AAC-induced cardiac dysfunction in rats

Echocardiographic data revealed that the EF (AAC: 48.77 ± 2.14% vs. sham: 68.91 ± 1.97%; $P < 0.001$) and FS (AAC:

25.94 ± 1.37% vs. sham: 40.08 ± 1.65%; $P < 0.001$) were decreased in the AAC group compared with sham group, whereas the LVID, d (AAC: 8.95 ± 0.17 mm vs. sham: 7.43 ± 0.19 mm; $P < 0.001$), LVID, s (AAC: 6.63 ± 0.17 mm vs. sham: 4.46 ± 0.20 mm; $P < 0.001$), LVvol; d (AAC: 443.40 ± 18.83 μl vs. sham: 293.50 ± 16.10 μl; $P < 0.001$), LVvol; s (AAC: 227.00 ± 13.06 μl vs. sham: 92.65 ± 8.81 μl; $P < 0.001$), LVPW, d (AAC: 2.22 ± 0.07 mm vs. sham: 1.92 ± 0.06 mm; $P < 0.01$), LVPW, s (AAC: 3.20 ± 0.10 mm vs. sham: 2.73 ± 0.06 mm; $P < 0.01$), IVS, d (AAC: 2.28 ± 0.08 mm vs. sham: 1.83 ± 0.04 mm; $P < 0.001$) and IVS, s (AAC: 3.23 ± 0.11 mm vs. sham: 2.80 ± 0.05 mm; $P < 0.001$) were increased in the AAC group (Fig. 1 b–g). Choline significantly increased the EF from 48.77 ± 2.14% to 62.80 ± 1.91% ($P < 0.001$), increased FS from 25.94 ± 1.37% to 35.25 ± 1.48% ($P < 0.01$), reduced LVID, d from 8.95 ± 0.17 mm to 7.46 ± 0.19 mm ($P < 0.001$), reduced LVID, s from 6.63 ± 0.17 mm to 4.82 ± 0.14 mm ($P < 0.001$), reduced LVvol; d from 443.40 ± 18.83 μl to 296.40 ± 16.74 μl ($P < 0.001$), reduced LVvol; s from 227.00 ± 13.06 μl to 109.70 ± 7.37 μl ($P < 0.001$), reduced LVPW, s from 3.20 ± 0.10 mm to 2.77 ± 0.08 mm ($P < 0.01$), reduced IVS, d from 2.28 ± 0.08 mm to 2.08 ± 0.03 mm ($P < 0.05$), and reduced IVS, s from 3.23 ± 0.11 mm to 2.84 ± 0.05 mm ($P < 0.01$) in the AAC group. Choline ameliorated the pathological changes and improved the cardiac function of AAC rats. No significant differences were observed between the sham group and choline-treated sham group.

Choline attenuated cardiac hypertrophy, fibrosis, and apoptosis in AAC rats

Pathological cardiac remodeling—characterized by cardiac hypertrophy, fibrosis, and apoptosis—progressively leads to heart failure. As shown in Fig. 2a, the heart size of AAC rats was larger than that of sham rats and was markedly reduced by choline. The area occupied by cardiomyocytes (AAC: 650.30 ± 5.06 μm^2 vs. sham: 363.90 ± 6.48 μm^2; $P < 0.001$) and cardiomyocyte cross-sectional diameter (AAC: 41.91 ± 0.36 μm vs. sham: 29.84 ± 0.38 μm; $P < 0.001$) were greater in the AAC group than in the sham group. Moreover, choline administration reduced the area occupied by cardiomyocytes from 650.30 ± 5.06 μm^2 to 457.40 ± 3.35 μm^2 ($P < 0.001$) and reduced cardiomyocyte cross-sectional diameter from 41.91 ± 0.36 μm to 34.15 ± 0.50 μm ($P < 0.001$) in the AAC group (Fig. 2a–c). In the AAC group, area of fibrosis was 3.76-fold that of sham group, and in the choline-treated AAC group, area of fibrosis was 1.31-fold that of sham group (Fig. 2d). Consistently, the ratios of heart weight to body weight (HW/BW; AAC: 3.24 ± 0.14 mg/g vs. sham: 2.65 ± 0.07 mg/g; $P < 0.001$) and left ventricular weight to body weight (LVW/BW; AAC: 2.64 ± 0.10 mg/g vs. sham: 2.10 ± 0.06 mg/g; $P < 0.001$) were markedly increased in AAC rats, with substantial reductions seen following choline administration (HW/BW: AAC + Choline, 2.69 ± 0.05 mg/g vs. AAC, 3.24 ± 0.14 mg/g, $P < 0.01$; LVW/BW: AAC + Choline, 2.35 ± 0.06 mg/g vs. AAC, 2.64 ± 0.10 mg/g, $P < 0.05$) (Fig. 2e, f), indicating that choline attenuated cardiac hypertrophy in AAC rats. Mean arterial pressure was higher in the AAC group than in the sham group (AAC: 128.90 ± 3.13 mmHg vs. sham: 98.31 ± 1.74 mmHg; $P < 0.001$), and a decrease in the mean arterial pressure was observed in the choline-treated AAC group (AAC + Choline, 107.20 ± 2.44 mmHg vs. AAC, 128.90 ± 3.13 mmHg, $P < 0.001$) (Fig. 2g).

Compared with the sham group, AAC-treated rats showed increased cardiac ANP, BNP, and β-MHC (markers of cardiac hypertrophy) expression, and choline ameliorated these alterations. Cardiac levels of ANP, BNP, and β-MHC in the AAC group were 2.58-, 4.33-, 3.88-fold higher than the sham group, respectively. In the AAC, rats were administrated choline, showing 1.26-, 2.30-, and 1.78-fold higher levels than in the sham group, respectively (Fig. 3a–d). There was no significant difference in ANP, BNP, or β-MHC expression between the sham and choline-treated sham groups. Western blotting revealed that α-MHC expression was decreased, while that of β-MHC was increased in the hearts of AAC rats. The expression of α-MHC was significantly enhanced by choline, while β-MHC expression was inhibited. The Western blotting results also showed that AAC decreased α-MHC/β-MHC in the heart compared with the sham group. Compared with the AAC group, the expression of α-MHC/β-MHC was increased in the choline-treated AAC group (Fig. 3e, f). Quantification of cardiac apoptosis by TUNEL assay indicated that apoptotic cells in the AAC rat hearts were 14.44-fold ($P < 0.001$) higher than the sham group, whereas choline reduced TUNEL-positive cells by 92.43% ($P < 0.001$) in the AAC group (Fig. 3g, h).

Choline not only normalized the diurnal variations of autonomic nervous functions, but also improved autonomic nervous balance in AAC rats

Diurnal variations in autonomic nervous activity underlie the pathogenesis of cardiovascular diseases [11]. We explored the effect of choline on circadian variation in the activity of the autonomic nervous system. Nocturnal patterns, in which the values of HR in the dark phase (ZT12-ZT24) were higher than those in the light phase (ZT0-ZT12), were observed (Fig. 4a). Both RMSSD and HF power in the light phase were higher than those in the dark phase (Fig. 4b, c). The LF and LF/HF ratio showed the opposite tendency to that of the HF (Fig. 4d, e). Coarctation of the abdominal aorta disrupted the circadian rhythms of HR, RMSSD, HF,

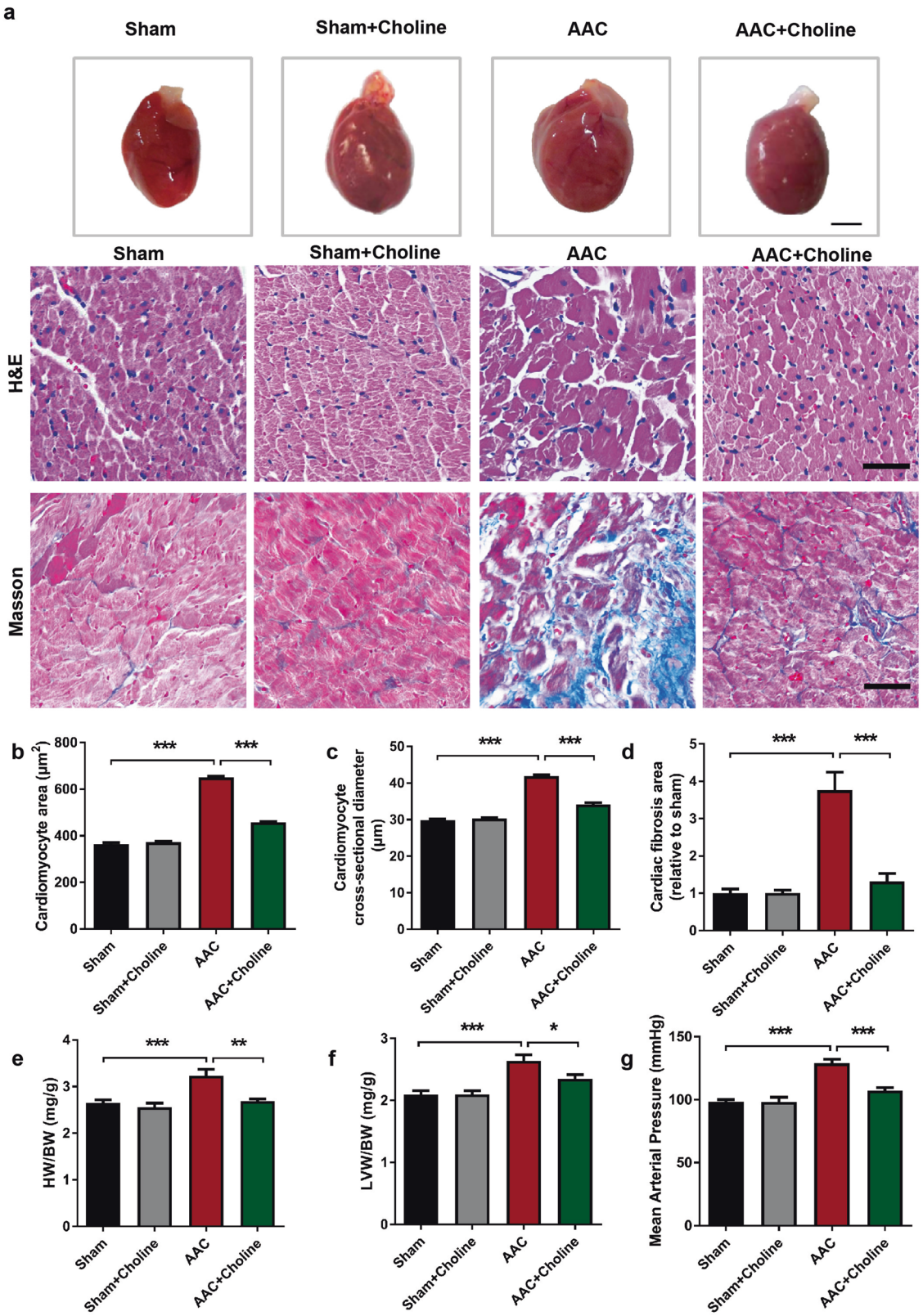

LF, and LF/HF; choline improved the diurnal variations in the levels of these markers. Moreover, when the overall 24 h levels were averaged, a significant increase was observed in HR (AAC: 365.3 ± 3.41 b.p.m vs. sham: 346.9 ± 3.13 b.p.m; $P < 0.01$) and a significant decrease in RMSSD (AAC: 1.63 ± 0.05 ms vs. sham: 2.60 ± 0.24 ms; $P < 0.01$) in AAC

◀ **Fig. 2 Choline attenuates cardiac remodeling in abdominal aortic coarctation (AAC) rats. a** Representative images of cardiac morphology, cardiomyocyte hypertrophy, and collagen deposition. Scale bars = 5 mm (top), 50 μm (middle) and 50 μm (bottom). **b**, **c** Area and cross-sectional diameter of cardiomyocytes in the left ventricle; $n = 8$ rats per group. **d** Area of cardiac fibrosis stained by Masson's trichrome; $n = 6$ rats per group. **e**, **f** Ratio of heart weight/body weight (HW/BW) and left ventricular weight (LVW)/BW; $n = 8$ rats per group. **g** Mean arterial pressure; $n = 8$ rats per group. Data are means ± SEM. $^{*}P < 0.05$, $^{**}P < 0.01$, $^{***}P < 0.001$. H&E, hematoxylin and eosin.

rats. In the frequency domain, HF power was lower (AAC: 12.13 ± 0.60% vs. sham: 16.13 ± 0.86%; $P < 0.01$), whereas the LF (AAC: 87.87 ± 0.60% vs. sham: 83.87 ± 0.86%; $P < 0.01$) and the LF/HF ratio (AAC: 7.51 ± 0.43 vs. sham: 5.41 ± 0.36; $P < 0.001$) were higher in the AAC group than in the sham group. Augmentation of HF (AAC + Choline: 15.73 ± 0.68% vs. AAC: 12.13 ± 0.60%; $P < 0.01$) and RMSSD (AAC + Choline: 2.53 ± 0.20 ms vs. AAC: 1.63 ± 0.05 ms; $P < 0.05$) and inhibition of HR (AAC + Choline: 347.9 ± 3.98 b.p.m vs. AAC: 365.3 ± 3.41 b.p.m; $P < 0.01$), LF (AAC + Choline: 84.27 ± 0.68% vs. AAC: 87.87 ± 0.60%; $P < 0.01$), and LF/HF (AAC + Choline: 5.46 ± 0.25 vs. AAC: 7.51 ± 0.43; $P < 0.001$) were observed after choline administration in the AAC group (Fig. 4a–e). Next, we explored the effect of choline on the serum ACh level. The serum level of ACh was significantly decreased in the AAC group compared with the sham group (AAC: 22.82 ± 0.59 μg/ml vs. sham: 27.43 ± 0.77 μg/ml; $P < 0.01$). Choline administration markedly increased the serum ACh level in the choline-treated AAC group (AAC + Choline: 27.59 ± 1.12 μg/ml vs. AAC: 22.82 ± 0.59 μg/ml; $P < 0.01$) (Fig. 4f). The serum level of CA and cardiac ACE activity were significantly increased in the AAC group compared with the sham group (CA: AAC, 215.76 ± 8.00 ng/ml vs. sham, 118.41 ± 13.41 ng/ml, $P < 0.001$; ACE: AAC, 0.36 ± 0.03 ng/mg vs. sham, 0.18 ± 0.01 ng/mg, $P < 0.001$) (Fig. 4g, h). Choline administration markedly reduced the CA level and cardiac ACE activity in the choline-treated AAC group (CA: AAC + Choline, 168.24 ± 3.97 ng/ml vs. AAC, 215.76 ± 8.00 ng/ml, $P < 0.05$; ACE: AAC + Choline, 0.23 ± 0.01 ng/mg vs. AAC, 0.36 ± 0.03 ng/mg, $P < 0.001$). Cardiac β1-AR protein levels and cardiac levels of cAMP (AAC: 0.22 ± 0.01 nmol/g vs. sham: 0.35 ± 0.01 nmol/g; $P < 0.001$) were significantly decreased in the AAC group, compared with the sham group. Choline administration significantly increased β1-AR protein expression and cardiac cAMP levels (AAC + Choline: 0.34 ± 0.03 nmol/g vs. AAC: 0.22 ± 0.01 nmol/g; $P < 0.001$) with respect to the AAC group (Fig. 4i, j). Therefore, AAC rats showed an altered circadian rhythm of autonomic nervous functions, significant decreases in cardiac vagal tone, and increases in sympathetic tone. Choline not only normalized the diurnal variations of autonomic nervous functions, but also improved autonomic nervous balance in AAC rats.

Effect of choline on the expression of circadian clock genes following AAC

In an AAC rat model, diurnal variation in HR, RMSSD, HF, and LF is abnormal, indicating that the circadian rhythm of autonomic nervous functions is altered in AAC rats. Many neurohumoral factors such as ACh, adrenaline, noradrenaline, and glucocorticoids, as well as renin-angiotensin activity and sympathetic activity, are affected in the AAC model [24–26]. As many of the potential zeitgebers are altered in the AAC model, and given that the morphology, function, and contractile performance of the heart are all altered in the AAC model, we explored whether the clock of the heart is also affected within this environment. We determined whether AAC led to significant changes in the circadian oscillations of clock genes in the rat heart and the effect of choline on the expression of heart clock components. We investigated the mRNA levels of seven key components of the clock mechanism (*Bmal1*, *Clock*, *Rev-erbα*, *Per1/2*, and *Cry1/2*) during the 24 h light/dark cycle (Fig. 5a). Figure 5 shows the circadian oscillations in the mRNA levels of *Bmal1*, *Clock*, *and Rev-erbα*. The mRNA levels of *Bmal1* and *Clock* had a circadian pattern of expression in the hearts of sham rats. The trough expression of *Bmal1* and *Clock* was at ZT12 (Fig. 5b, c). Expression *of Rev-erbα* underwent a striking circadian rhythm in the heart, with peak expression at ZT6 and trough expression at ZT18 (Fig. 5d). Oscillations in these three circadian clock genes were significantly attenuated in hearts from the AAC group vs. the sham group. Furthermore, choline improved the rhythms and significantly increased *bmal1* expression at ZT0, 6, 18, and 24; increased *Clock* expression at ZT0, 6, and 18; and increased *Rev-erbα* expression at ZT0, 6, and 24 in AAC hearts (Fig. 5b–d). There were no significant differences in the levels of *Bmal1*, *Clock*, and *Rev-erbα* expression between sham and choline-treated sham hearts at the same time points.

The transcripts encoding *Per1* and *Per2* showed circadian patterns of expression in sham hearts. *Per1 and Per2* had peak expression at ZT12 and trough expression at ZT0 in sham hearts (Fig. 6a, b). The transcripts encoding *Cry1* and *Cry2* showed circadian rhythmicity of expression in hearts from sham rats. Moreover, this rhythmicity was comparable between the two *Cry* isoforms, with peaks at ZT18 and troughs at ZT6 (Fig. 6c, d). AAC not only altered the rhythms, but also increased the expression levels of *Per1/2* and *Cry1/2* in the heart. Furthermore, choline improved the rhythms and markedly decreased *Per1*

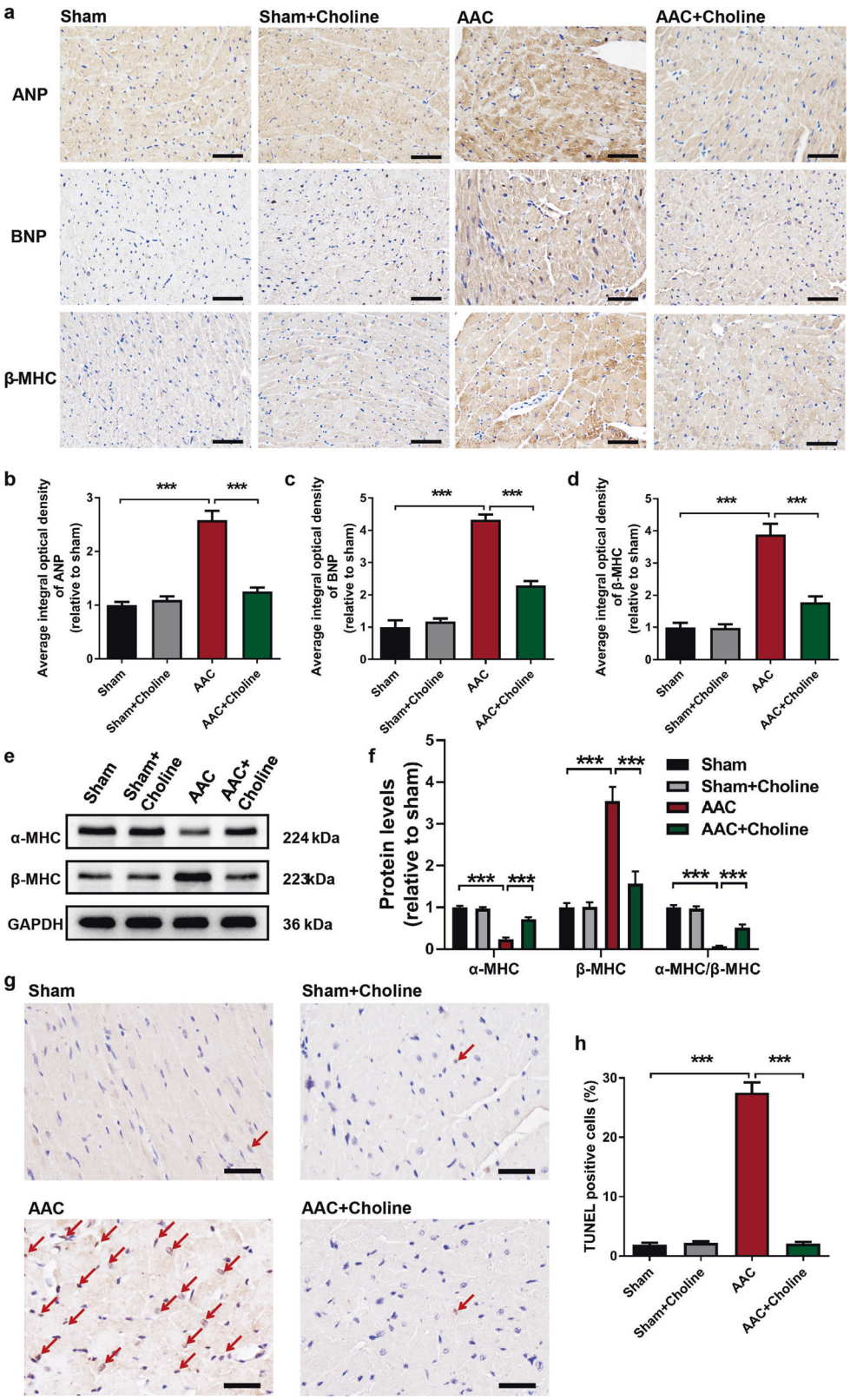

Fig. 3 Choline attenuates cardiac hypertrophy and apoptosis in abdominal aortic coarctation (AAC) rats. a–d Immunohistochemical analysis of atrial natriuretic peptide (ANP), brain natriuretic peptide (BNP), and β-myosin heavy chain (β-MHC) expression in heart tissues. Scale bar = 50 μm. Representative images (**e**) and summarized data (**f**) of Western blotting analysis of α-MHC and β-MHC in heart tissues. **g** Representative images of terminal deoxynucleotidyl transferase-mediated dUTP nick-end labeling (TUNEL) staining. **h** Quantification of TUNEL signal. Scale bar = 50 μm. Red arrows indicate TUNEL-positive cells. Data are means ± SEM ($n = 6$ rats per group). $^{***}P < 0.001$.

expression at ZT12; decreased *Per2* expression at ZT6, 12, and 18; decreased *Cry1* expression at ZT0, 6, 12 and 24; and decreased *Cry2* expression at ZT12 in AAC hearts (Fig. 6a–d). There were no significant differences in the levels of *Per1/2* and *Cry1/2* expression between sham and choline-treated sham hearts at the same time points.

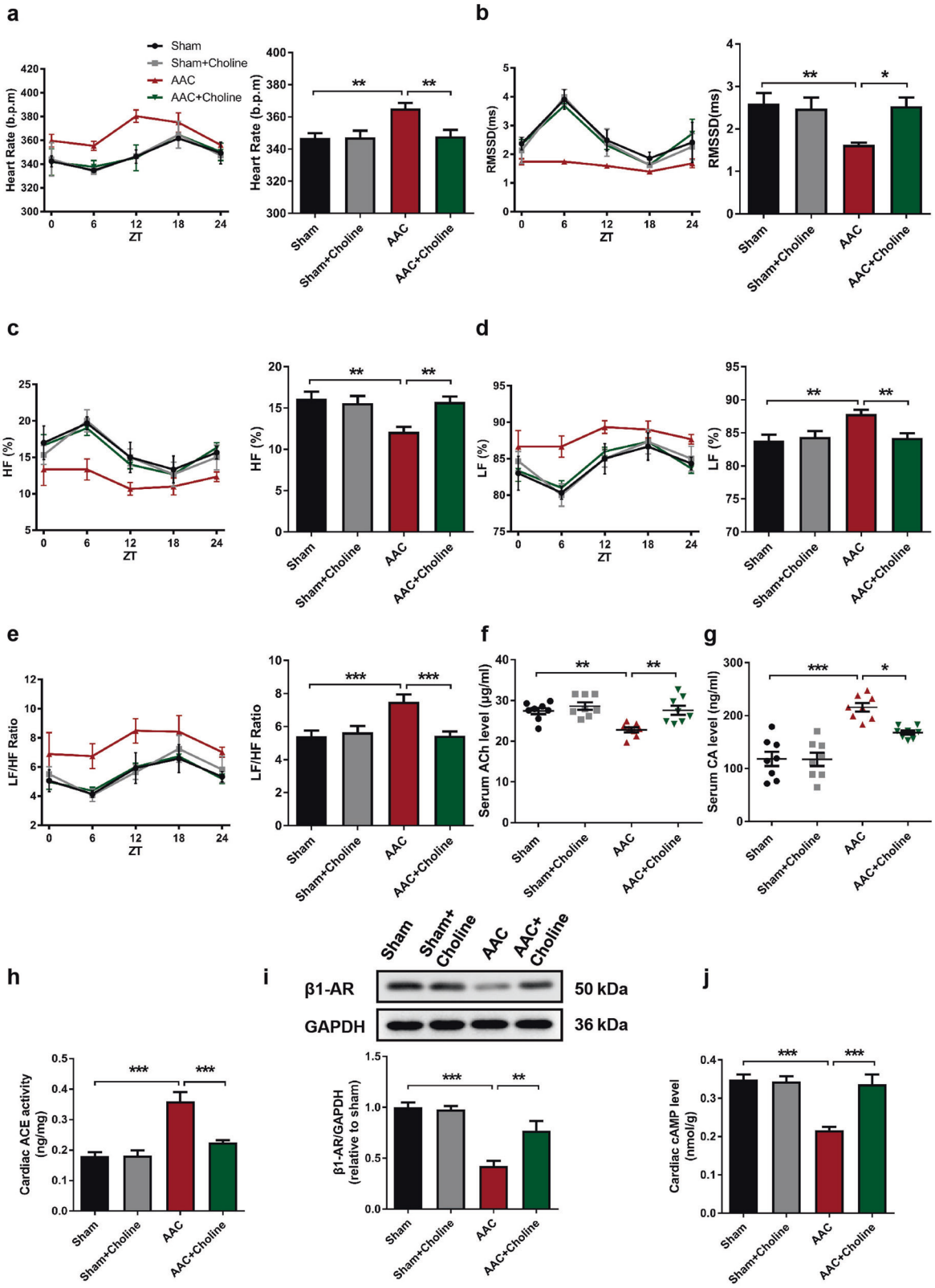
a
Sham
Sham+Choline
AAC
AAC+Choline
Heart Rate (b.p.m)
ZT
b
RMSSD(ms)
c
HF (%)
d
LF (%)
e
LF/HF Ratio
f
Serum ACh level (μg/ml)
g
Serum CA level (ng/ml)
h
Cardiac ACE activity (ng/mg)
i
β1-AR
GAPDH
50 kDa
36 kDa
β1-AR/GAPDH (relative to sham)
j
Cardiac cAMP level (nmol/g)

◀ **Fig. 4 Choline not only normalized the diurnal variations of autonomic nervous functions, but also improved autonomic nervous balance in abdominal aortic coarctation (AAC) rats.** Circadian rhythm of heart rate (**a**), root mean square successive difference (RMSSD) (**b**), high frequency (HF) (**c**), low frequency (LF) (**d**), and absolute values of the LF/HF ratio (**e**) ($n = 3$ rats per group per time point). To provide a 24 h overall mean level, the data over a 24 h period in each group were averaged and plotted ($n = 15$). **f** Serum level of acetylcholine (ACh). $n = 8$ rats per group. **g** Serum level of catecholamine (CA). $n = 8$ rats per group. **h** Cardiac angiotensin converting enzyme (ACE) activity. $n = 8$ rats per group. **i** Cardiac β1-adrenergic receptor (β1-AR) level. $n = 6$ rats per group. **j** Cardiac cyclic adenosine monophosphate (cAMP) level. $n = 8$ rats per group. Data are means ± SEM. $^{*}P < 0.05$, $^{**}P < 0.01$, $^{***}P < 0.001$.

Choline downregulated the protein levels of STIM1, Orai1, and TRPC6 and attenuated calcium overload in hypertrophied cardiomyocytes

In cardiac remodeling, an increase in cytosolic calcium can be caused by excessive calcium entry into the cytosol, which includes STIM1/Orai1-mediated SOCE and TRPC6-mediated ROCE (Fig. 7a). We examined the protein levels of STIM1 and Orai1, which are believed to form the SOCC responsible for SOCE, as well as the level of TRPC6, which contributes to forming ROCC. Western blotting experiments showed that the protein levels of STIM1, Orai1, and TRPC6 in rat heart tissues were 1.99-fold ($P < 0.01$), 2.18-fold ($P < 0.001$), and 1.55-fold ($P < 0.001$) higher, respectively, in the AAC group relative to the sham group; whereas choline reduced protein levels of STIM1, Orai1, and TRPC6 by 43.72% ($P < 0.01$), 40.83% ($P < 0.01$), and 19.35% ($P < 0.05$), respectively, in the AAC group (Fig. 7b, c). Therefore, AAC markedly upregulated the levels of the proteins that participate in the formation of SOCC (e.g., STIM1 and Orai1) and ROCC (e.g., TRPC6), and choline decreased the protein levels of STIM1, Orai1, and TRPC6 in AAC rats.

Given the protective role of choline in vivo in the classic AAC model, we next tested the effect of choline in blocking cellular remodeling in response to neurohormonal stress. Ang II is a primary effector peptide of the RAS and directly promotes cardiac cell death, hypertrophy, and remodeling. Therefore, we investigated whether choline could ameliorate Ang II-induced cardiomyocyte remodeling by alleviating calcium dyshomeostasis. Ang II-induced cardiomyocyte hypertrophy was demonstrated by increased expression of hypertrophic markers (ANP and β-MHC) and these increases were prevented by choline (data not shown). Ca^{2+} fluorescence intensity measured by Fluo-4 staining in the Ang II-treated group was 1.67-fold ($P < 0.001$) higher than the control group (Fig. 7d, e). In contrast, choline attenuated the Ca^{2+} fluorescence intensity by 40.12% ($P < 0.001$) relative to the Ang II group. Choline had no significant effect on the intracellular Ca^{2+} level of control cells. Figure 7f shows representative Fluo-4 images acquired before and during SOCE. The SOCE-induced increase in $[Ca^{2+}]_i$ (change in Fluo-4 fluorescence ratio F/F_0) in Ang II-treated NRVCs was significantly attenuated by choline (Ang II + Choline: 2.42 ± 0.15 vs. Ang II: 3.62 ± 0.22; $P < 0.001$) (Fig. 7g). Extracellular application of the membrane-permeable diacylglycerol analogue, OAG, directly activates ROCC and induces ROCE. OAG-induced ROCE in Ang II-treated NRVCs was significantly higher compared with control NRVCs (Ang II: 2.53 ± 0.14 vs. control: 1.91 ± 0.09; $P < 0.001$) (Fig. 7h, i). Choline had no significant effect on ROCE in control cells, but led to suppression of ROCE in Ang II-treated NRVCs (Ang II + Choline: 1.88 ± 0.09 vs. Ang II: 2.53 ± 0.14; $P < 0.001$). The protein levels of STIM1, Orai1, and TRPC6 in Ang II-induced hypertrophic cardiomyocytes were 2.68-fold ($P < 0.001$), 2.00-fold ($P < 0.001$), and 1.50-fold ($P < 0.001$) higher than the controls, respectively; choline decreased the protein levels of STIM1, Orai1, and TRPC6 by 47.76% ($P < 0.01$), 40.50% ($P < 0.01$), and 16.00% ($P < 0.05$), respectively, in Ang II-treated cells (Fig. 7j, k).

Discussion

Circadian rhythm disruption and calcium dyshomeostasis contribute to the development of cardiac remodeling and heart failure. We evaluated the effect of choline on cardiac remodeling, circadian rhythm disruption, and SOCC/ROCC-mediated calcium dyshomeostasis in AAC rats. The findings can be summarized as follows. (1) AAC altered the circadian rhythms of the transcript levels of the seven major components of the mammalian clock (*Bmal1*, *Clock*, *Rev-erbα*, *Per1/2*, and *Cry1/2*) in the rat heart. AAC also upregulated the protein levels of SOCC/ROCC (STIM1, Orai1, and TRPC6) in the rat heart. (2) Choline ameliorated circadian rhythm disruption, reduced the upregulated protein levels of STIM1, Orai1, and TRPC6, and alleviated cardiac dysfunction and remodeling (evidenced by attenuated cardiac hypertrophy, fibrosis, and apoptosis) in AAC rats. (3) In vitro, choline ameliorated calcium overload, downregulated STIM1, Orai1, and TRPC6, and inhibited TG-induced SOCE and OAG-induced ROCE in Ang II-treated cardiomyocytes (Fig. 8). Collectively, these data show that amelioration of circadian rhythm disruption and attenuation of intracellular calcium dyshomeostasis may be important mechanisms underlying the cardioprotective effect of choline. To the best of our knowledge, this is the first report on the protective effect of choline on AAC-induced circadian rhythm disruption and defects in Ca^{2+}-handling proteins (SOCC/ROCC).

Cardiac remodeling is characterized by overactivity of the sympathetic nervous system and the RAS and

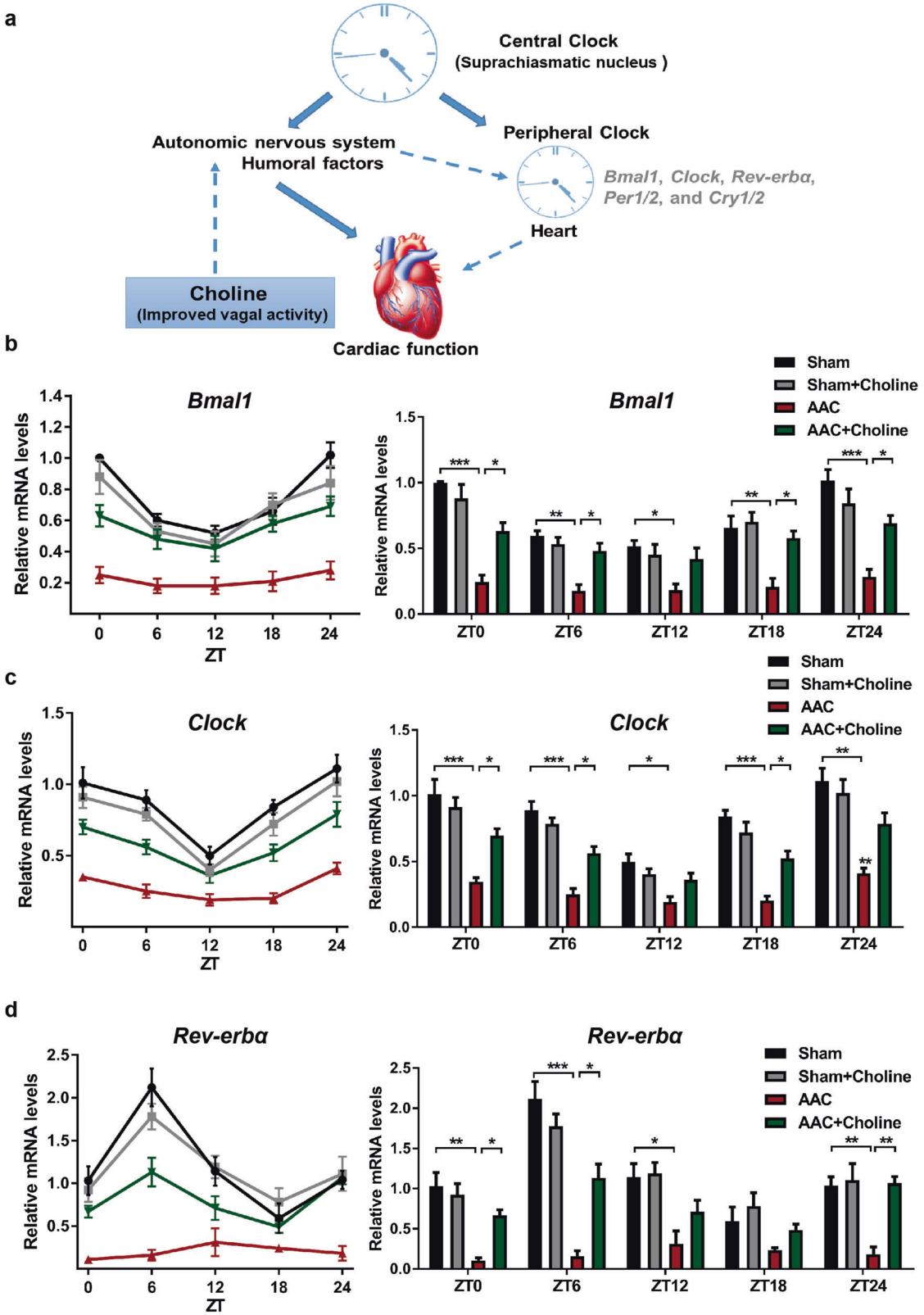

Fig. 5 Effect of choline on the circadian expression of genes regulating clock machinery in the heart of abdominal aortic coarctation (AAC) rats. a Improvement by choline of the circadian clock rhythms suggests that the autonomic nervous system, or a neurohumoral factor under its direct or indirect control, acts as a zeitgeber in the heart. Relative expression levels of *Bmal1* (**b**), *Clock* (**c**), and *Rev-erbα* (**d**) in the heart at zeitgeber time (ZT) 0, 6, 12, 18, and 24. Data are means ± SEM ($n = 3$ rats per group per time point). $^{*}P < 0.05$, $^{**}P < 0.01$, $^{***}P < 0.001$.

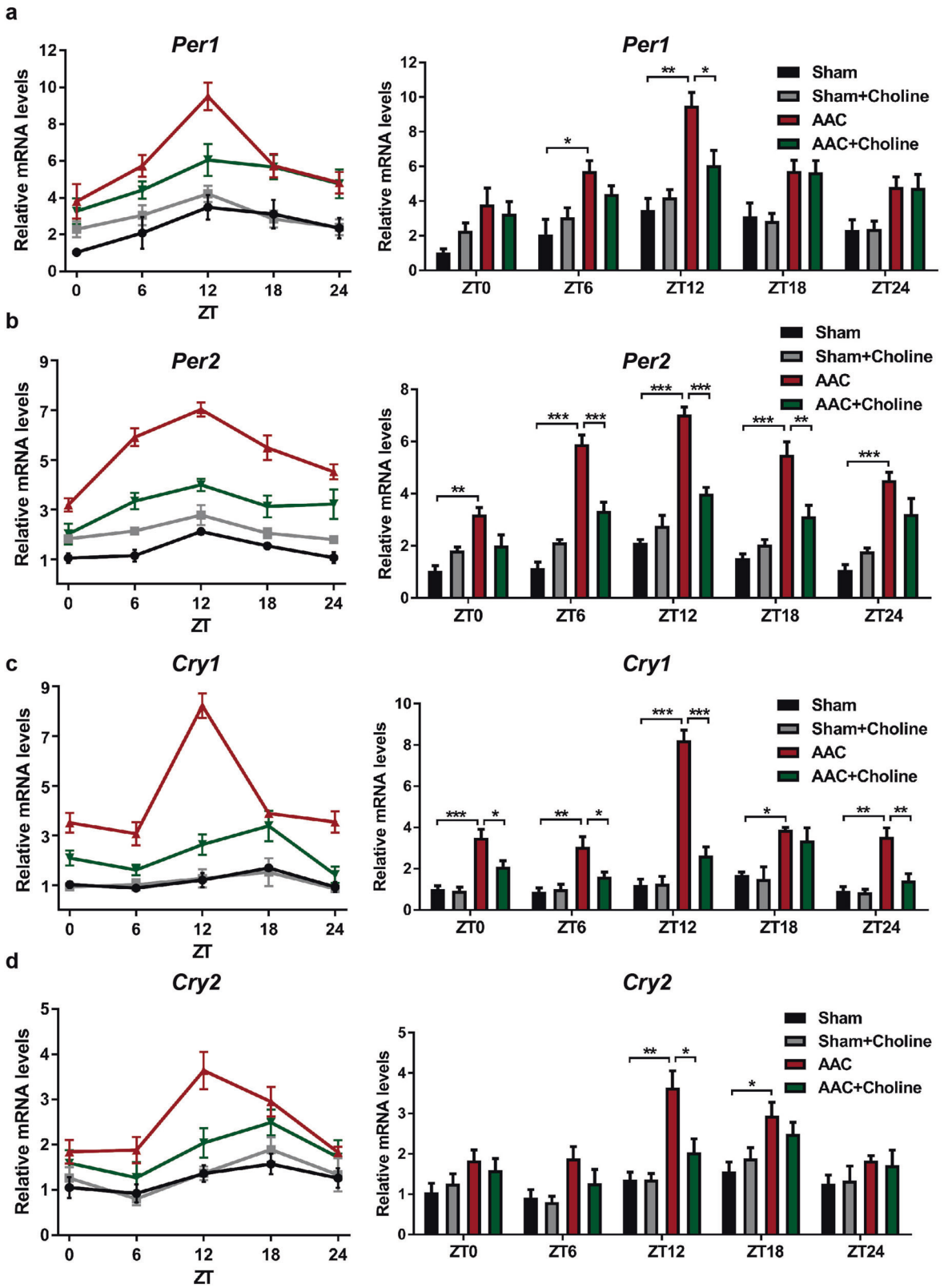

Fig. 6 Effect of choline on the circadian expression of clock genes in hearts of abdominal aortic coarctation (AAC) rats. Relative expression levels of *Per1* (**a**), *Per2* (**b**), *Cry1* (**c**), and *Cry2* (**d**) in hearts at zeitgeber time (ZT) 0, 6, 12, 18, and 24. Data are means ± SEM ($n = 3$ rats per group per time point). $^{*}P < 0.05$, $^{**}P < 0.01$, $^{***}P < 0.001$.

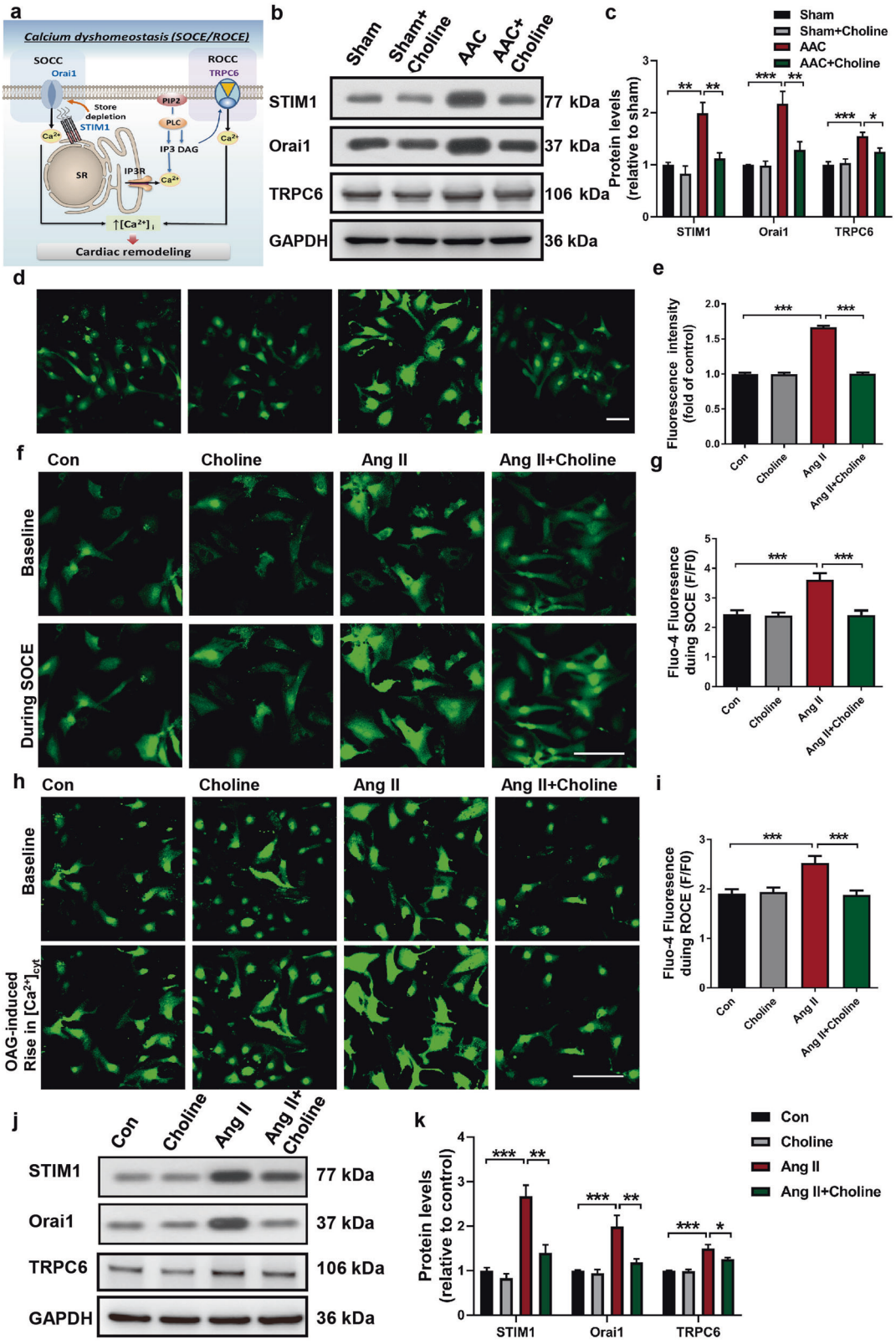

suppressed activity of the vagal (parasympathetic) nervous system. In the present study, we observed that choline significantly reduced AAC-induced increases in blood pressure, ACE activity, and serum levels of CA, and upregulated the AAC-induced decreases in β1-AR protein expression and cardiac cAMP levels. These results suggest

◀ **Fig. 7 Choline downregulates the protein levels of stromal interaction molecule 1 (STIM1), Orai1, and transient receptor potential canonical 6 (TRPC6) and attenuates calcium overload in hypertrophied cardiomyocytes. a** In cardiac remodeling, an increase in cytosolic calcium can be caused by excessive calcium entry into the cytosol, which includes STIM1/Orai1-mediated store-operated Ca^{2+} entry (SOCE) and TRPC6-mediated receptor-operated Ca^{2+} entry (ROCE). Representative images (**b**) and summarized data (**c**) of Western blotting analysis of STIM1, Orai1, and TRPC6 in the hearts of sham and abdominal aortic coarctation (AAC) rats treated with choline or saline. Data are means ± SEM ($n = 5$ rats per group). $^{*}P < 0.05$, $^{**}P < 0.01$, $^{***}P < 0.001$. **d**, **e** Choline alleviated angiotensin II (Ang II)-induced intracellular Ca^{2+} overload in neonatal rat ventricular myocytes (NRVMs). Scale bar = 50 μm. Data are means ± SEM ($n = 300$ cells from six independent experiments). $^{***}P < 0.001$. **f**, **g** Intracellular $[Ca^{2+}]_i$ changes during SOCE in NRVMs. Representative Fluo-4 images and summarized Fluo-4 signal intensity data acquired before and during SOCE. Scale bar = 100 μm. Data are means ± SEM ($n = 216$–233 cells from four independent experiments). $^{***}P < 0.001$. **h**, **i** Intracellular $[Ca^{2+}]_i$ changes during ROCE in NRVMs. Representative images and summarized data showing 1-oleoyl-2-acetyl-sn-glycerol (OAG, an analog of diacylglycerol)-induced rise in $[Ca^{2+}]_{cyt}$. Scale bar = 100 μm. Data are means ± SEM ($n = 161$–231 cells from four independent experiments). $^{***}P < 0.001$. **j**, **k** Representative images and summarized data of Western blotting analysis of STIM1, Orai1, and TRPC6 in NRVMs. Data are means ± SEM ($n = 5$ independent experiments). $^{*}P < 0.05$, $^{**}P < 0.01$, $^{***}P < 0.001$.

that choline has an indirect effect due to the modulation of blood pressure and neuroendocrine signaling. These results are consistent with those of our previous study, in which improving vagal activity by pyridostigmine, a cholinesterase inhibitor, inhibited cardiac remodeling induced by pressure overload via suppressing RAS activation [26]. As a precursor for biosynthesis of the vagal nerve neurotransmitter ACh, choline has a marked protective effect against cardiac remodeling, possibly by augmenting vagal activity and suppressing chronic overactivity of the RAS and the sympathetic nervous system.

In addition, a previous study has demonstrated the additional beneficial effects obtained from the combination of pharmacological restoration of vagal activity by donepezil and inhibition of RAS by losartan for the treatment of heart failure, indicating that improved vagal activity exerts a direct cardioprotective effect. An acetylcholinesterase inhibitor, donepezil, is effective in further ameliorating cardiac dysfunction and improving long-term survival when administered in combination with a specific Ang II receptor blocker, losartan in rats with heart failure. Compared with the losartan alone group, the combination of donepezil and losartan group showed a significantly lower HR, lower plasma CA levels, and lower cardiac Ang II concentrations [27]. Therefore, choline improved vagal activity and may exert a direct effect, with potential pharmacological synergism when combined with an ACE inhibitor/Ang II receptor blocker.

Heart rate reduction is a possible treatment mechanism involved in the direct effect of choline. In the present study, vagal activation by choline markedly reduced the HR. A prolonged cardiac cycle is beneficial in enhancing and maintaining cardiac function, by reducing myocardial oxygen consumption, elevating coronary flow, and elevating ventricular filling volume [28]. Therefore, the bradycardic effect seen in the choline-treated AAC group may be one of the important factors for ameliorating cardiac dysfunction. In addition to the above-mentioned mechanisms, the attenuation of defects in Ca^{2+}-handling proteins may be another important mechanism for choline-induced cardiac protection. Our in vitro study showed that choline ameliorated calcium overload, downregulated STIM1, Orai1, and TRPC6, and inhibited TG-induced SOCE and OAG-induced ROCE in Ang II-treated cardiomyocytes, suggesting that choline could regulate calcium homeostasis of cardiomyocytes directly and has a direct protective effect on cardiomyocytes. Thus, attenuation of enhanced expression of SOCC/ROCC and improvement of calcium homeostasis by choline may partly account for the suppression of cardiac remodeling and cardiac dysfunction. The beneficial effects of choline may include its direct effect and indirect effect due to the modulation of blood pressure and neuroendocrine signaling. The combination of choline and an ACEI/a β-blocker as a therapy for cardiac remodeling and heart failure should be examined in a further study.

The circadian rhythm plays an important role in cardiovascular physiology; disruption of the rhythm can result in the development and progression of cardiovascular diseases. Multiple cardiovascular variables in humans exhibit time-of-day variation, including blood pressure, HR, and activity of the autonomic nervous system [29, 30]. Moreover, the occurrence of adverse cardiovascular events, including myocardial infarction, stroke, and sudden cardiac death have daily patterns, striking most frequently in the morning [30]. Furthermore, chronic disruptions of the circadian clock, as with night-shift work, significantly increase the risk of cardiovascular disease. A recent study of shift workers indicated that circadian misalignment increased 24 h blood pressure and the levels of inflammatory markers such as tumor necrosis factor-α, C-reactive protein, and interleukin-6 [31]. In this study, the efferent cardiac vagal activity (estimated from RMSSD and HF power) in the light phase was significantly higher than that in the dark phase. This suggests that vagal nervous activity is predominant in the light phase in rats. Interestingly, coarctation of the abdominal aorta in rats disrupted the circadian rhythms of HR, RMSSD, HF, LF, and LF/HF; choline improved the diurnal variations in the levels of these markers. Commonly reported measures of vagally mediated HRV include the RMSSD—a time-domain measure—and the HF component of HRV. Moreover, the ratio of LF to HF (LF/HF) has been

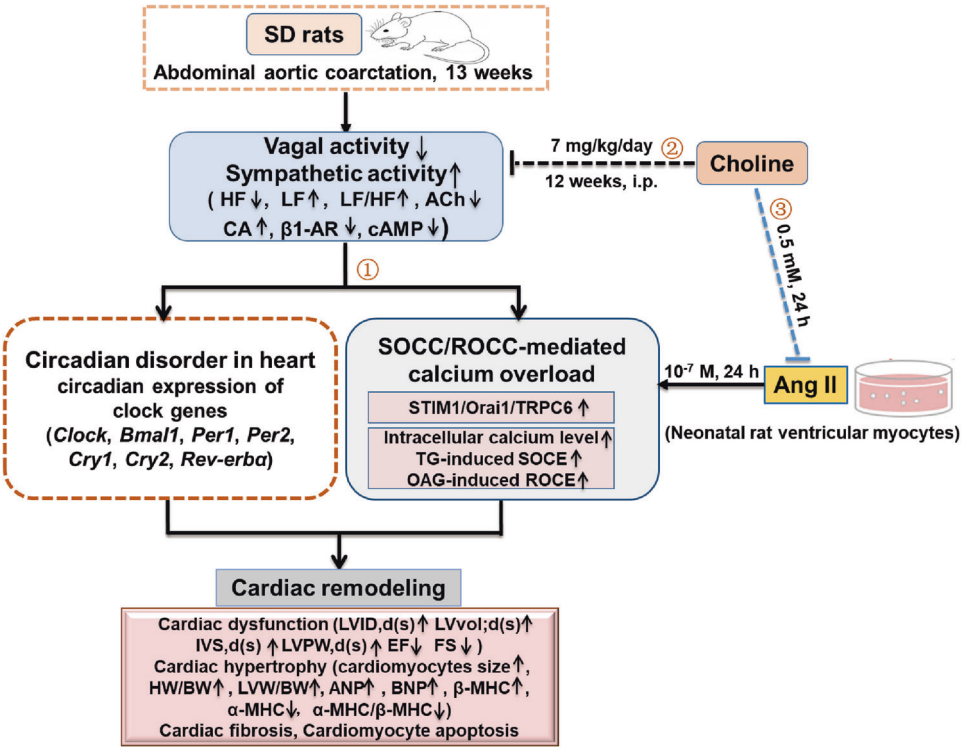

Fig. 8 Illustration of the proposed mechanism underlying the cardioprotective effect of choline. (1) Abdominal aortic coarctation (AAC) altered the circadian rhythms of the transcript levels of the seven major components of the mammalian clock (*Bmal1*, *Clock*, *Rev-erbα*, *Per1/2*, and *Cry1/2*) in the rat heart. AAC also upregulated the protein levels of store-operated Ca^{2+} channels (SOCC)/receptor-operated Ca^{2+} channels (ROCC) (stromal interaction molecule 1 [STIM1], Orai1, and transient receptor potential canonical 6 [TRPC6]) in the rat heart. (2) Choline improved autonomic nervous balance, ameliorated circadian rhythm disruption, reduced the upregulated protein levels of STIM1, Orai1, and TRPC6, and alleviated cardiac dysfunction and remodeling (evidenced by attenuated cardiac hypertrophy, fibrosis, and apoptosis) in AAC rats. (3) In vitro, choline ameliorated calcium overload, downregulated STIM1, Orai1, and TRPC6, and inhibited thapsigargin (TG)-induced store-operated Ca^{2+} entry (SOCE) and 1-oleoyl-2-acetyl-sn-glycerol (OAG)-induced receptor-operated Ca^{2+} entry (ROCE) in angiotensin II (Ang II)-treated cardiomyocytes. Collectively, amelioration of circadian rhythm disruption and attenuation of intracellular calcium dyshomeostasis may be important mechanisms underlying the cardioprotective effect of choline.

widely used to reflect the sympathovagal balance (in which an increased LF/HF ratio indicates sympathetic dominance, whereas reduction in this ratio reflects parasympathetic dominance) [32]. However, it should be noted that the physiological interpretation of LH/HF has to be considered with caution, as it is unclear and likely underestimates the complex interactions between the sympathetic and parasympathetic regulation of HR [33].

The central clock orchestrates the phase of each peripheral clock through the autonomic nervous system or humoral factors [11]. Light is the classical zeitgeber of the central clock, while neurohumoral factors appear to be the zeitgebers for peripheral clocks [11, 34]. In the AAC rat model, the circadian pattern of HR, RMSSD, HF and LF are abnormal, indicating that the circadian rhythm of autonomic nervous functions is altered in AAC rats. Many neurohumoral factors such as ACh, adrenaline, noradrenaline, and glucocorticoids, as well as renin-angiotensin activity and sympathetic activity, are affected in the AAC model [24–26]. Few studies have explored the circadian clock of the heart in the context of AAC and heart failure. Given that many of the potential zeitgebers are altered in the AAC model, we investigated whether AAC would change the circadian clock of the heart and the implications of circadian oscillators in response to vagal nervous system activation in the heart. The results showed that oscillations in circadian clock genes (including *Bmal1*, *Clock*, and *Rev-erbα*) in the heart were significantly attenuated in the AAC group vs. the sham group. AAC not only altered rhythms, but also increased the expression levels of *Per1/2* and *Cry1/2* in the heart. These changes in the circadian clock of the heart are probably due to changes in circulating zeitgebers during cardiac remodeling. The peripheral heart clock has therefore lost normal synchronization with its environment. Furthermore, choline improved the rhythms of these circadian clock genes and increased the expression of *Bmal1*, *Clock*, and *Rev-erbα* in the AAC heart. Choline also improved the circadian rhythm and markedly decreased the expression of

Per1/2 and *Cry1/2* in the AAC heart. To the best of our knowledge, this is the first report of the protective effect of choline on AAC-induced circadian rhythm disruption. *Bmal1* and *Per2* expression reportedly show a circadian pattern with opposing phases in bone. Isoproterenol-mediated chronic activation of β-adrenergic receptor signaling increased *Per2* expression and decreased *Bmal1* expression in bone, indicating that the sympathetic nervous system regulates bone remodeling and mediates clock genes in part via β-adrenergic receptor in osteoblasts [35]. These changes in the circadian clock of the heart are probably due to changes in circulating zeitgebers such as neurohumoral zeitgebers [34], supporting a link between the vagal nervous system and changes in the circadian clock in heart diseases. Further studies should address the causal role of the circadian clock in the pathophysiology of cardiovascular diseases using genetically modified mouse models, such as the circadian clock mutant mouse. Disruptions of the molecular clock in animals cause cardiovascular diseases, underscoring the importance of circadian rhythms. Knockout of Bmal1 in mice results in dilated cardiomyopathy [36] and cardiomyocyte-specific knockout of Bmal1 eliminates much of the rhythmic transcriptome, decreases cardiac function, and eventually results in heart failure in mice [37]. Disrupting the key circadian regulator Clock in mice leads to age-dependent cardiac hypertrophy and fibrosis [38]. These findings suggest an essential role for the circadian clock in cardiomyocyte homeostasis. Our results showed that choline improved the expression and rhythms of these circadian clock genes, suggesting choline-mediated improvement of vagal activity to a novel therapeutic target for cardiovascular disorders.

In heart failure, an increase in cytosolic calcium can be caused by reduced calcium efflux from the cytosol or excessive calcium influx into the cytosol. Excessive calcium influx is caused by defects in the voltage-gated L-type calcium channel, plasmalemmal Na^+/Ca^{2+} exchangers, and SOCE [39]. STIM1 and Orai1, the key mediators of SOCE, are present in cardiac myocytes and their abundance and SOCE activity increases in cardiac disease models [15, 40]. This increase has been linked to maladaptive cardiac hypertrophy [15, 16]. Hypertrophied myocytes upregulated STIM1 expression, which correlated with aberrant Ca^{2+}-handling, and STIM1–Orai-mediated Ca^{2+} influx contributes to both the induction of pathological hypertrophy and the electromechanical derangements of the hypertrophied heart [12]. TRPC channels are expressed at very low levels in normal cardiac myocytes, but their expression is increased in pathological hypertrophy and heart failure [41]. TRPC6 is the major component of ROCC responsible for ROCE [14]. TRPC6-formed ROCCs can be opened by the membrane-permeable diacylglycerol analogue, OAG, or by other signaling messengers involved in the G-protein signaling pathway. Cardiac overexpression of TRPC6 in transgenic mice resulted in pathological cardiac remodeling [42]. TRPC6 blockade shows therapeutic and prophylactic potential for pathological cardiac hypertrophy and remodeling [43]. Consistent with previous reports, our results showed that the protein levels of SOCC (STIM1/Orai1) and ROCC (TRPC6) were increased in hearts from AAC rats and Ang II-treated cardiomyocytes. Calcium dyshomeostasis, especially pathological increases in intracellular Ca^{2+} (Ca^{2+} overload), is a pivotal event during the progression of cardiac hypertrophy and heart failure [44]. A recent study also showed elevated cytosolic Ca^{2+} in the AAC model [45]. Based on these results, upregulated protein expression of SOCC and ROCC may contribute, at least in part, to calcium dyshomestasis in the AAC model. Furthermore, the functional data are consistent with the results of Western blotting; i.e., that the amplitudes of TG-induced SOCE and OAG-induced ROCE are greater in Ang II-induced hypertrophic cardiomyocytes than in control cells. Intriguingly, choline decreased the protein levels of STIM1, Orai1, and TRPC6 in the hypertrophied myocardium of rats and in Ang II-treated cells. Choline also attenuated Ang II-induced myocyte hypertrophy and calcium overload, possibly by decreasing TG-induced SOCE and OAG-induced ROCE, suggesting that modulation of SOCC and ROCC is important for the cardioprotective effect of choline.

Autonomic imbalance characterized by vagal (parasympathetic) withdrawal and sympathetic predominance is associated with the development of hypertrophy and heart failure. As the ACh precursor, choline exerts a marked protective effect on the injured heart by correcting abnormal DNA methylation [8] and regulating metabolic remodeling and the mitochondrial unfolded-protein response [18]. However, the effect of choline on circadian rhythms and calcium homeostasis in pathological cardiac remodeling have not been characterized. Our results demonstrated that choline not only normalized the diurnal variations of autonomic nervous functions but also improved the vagal-activity parameters of AAC rats, suggesting that neuronal cholinergic mechanisms contributed in part to the protective effect of choline on cardiac remodeling in vivo. In addition, choline ameliorated the alterations in the circadian oscillations of clock genes and reduced the upregulated protein levels of STIM1, Orai1, and TRPC6 in the heart of AAC rats. Therefore, the cardioprotective effects of choline may be correlated with the amelioration of circadian rhythm disruption and attenuation of intracellular calcium dyshomeostasis in a pathological setting.

In conclusion, choline attenuated AAC-induced cardiac remodeling and cardiac dysfunction, which was related to amelioration of circadian rhythm disruption and attenuation of the enhanced expression of SOCC/ROCC. AAC-induced alterations of the circadian clock in the heart may disrupt the

synchronicity between the stimulus and responsiveness of the system, thus contributing to tissue remodeling and, ultimately, development of heart failure. Improvement by choline of the circadian clock rhythms suggests that the autonomic nervous system, or a neurohumoral factor under its direct or indirect control, acts as a zeitgeber in the heart. These results indicate that there is novel potential for targeting the circadian mechanism to attenuate cardiac remodeling and heart failure. Modulation of vagal activity by choline targeting the circadian rhythm and calcium homeostasis shows therapeutic potential for heart diseases.

Data availability

All data generated or analyzed during this study are included in this published article.

Funding This work was supported by the grants from the National Natural Science Foundation of China (No. 81872868, No. 81970221, No. 81770293) and China Postdoctoral Science Foundation (2019M663754).

Author contributions XH and W-JZ performed study concept and design; XH, SY and JD conducted experiments; XH, SY, QW, W-JZ provided acquisition, analysis and interpretation of data, and statistical analysis; XH and W-JZ drafted paper. All authors read and approved the final paper.

Compliance with ethical standards

Conflict of interest The authors declare no competing interests.

Publisher's note Springer Nature remains neutral with regard to jurisdictional claims in published maps and institutional affiliations.

References

1. Wang HJ, Wang W, Cornish KG, Rozanski GJ, Zucker IH. Cardiac sympathetic afferent denervation attenuates cardiac remodeling and improves cardiovascular dysfunction in rats with heart failure. Hypertension. 2014;64:745–55.
2. Heusch G, Libby P, Gersh B, Yellon D, Böhm M, Lopaschuk G, et al. Cardiovascular remodelling in coronary artery disease and heart failure. Lancet. 2014;383:1933–43.
3. Floras JS, Ponikowski P. The sympathetic/parasympathetic imbalance in heart failure with reduced ejection fraction. Eur Heart J. 2015;36:1974–1982b.
4. Normand C, Kaye DM, Povsic TJ, Dickstein K. Beyond pharmacological treatment: an insight into therapies that target specific aspects of heart failure pathophysiology. Lancet. 2019;393:1045–55.
5. He X, Zhao M, Bi X, Sun L, Yu X, Zhao M, et al. Novel strategies and underlying protective mechanisms of modulation of vagal activity in cardiovascular diseases. Br J Pharmacol. 2015;172:5489–5500.
6. Liu L, Zhao M, Yu X, Zang W. Pharmacological modulation of vagal nerve activity in cardiovascular diseases. Neurosci Bull. 2019;35:156–66.
7. Schwartz PJ, De Ferrari GM, Sanzo A, Landolina M, Rordorf R, Raineri C, et al. Long term vagal stimulation in patients with advanced heart failure: first experience in man. Eur J Heart Fail. 2008;10:884–91.
8. Liu L, He X, Zhao M, Yang S, Wang S, Yu X, et al. Regulation of DNA methylation and 2-OG/TET signaling by choline alleviated cardiac hypertrophy in spontaneously hypertensive rats. J Mol Cell Cardiol. 2019;128:26–37.
9. Lu XZ, Bi XY, He X, Zhao M, Xu M, Yu XJ, et al. Activation of M3 cholinoceptors attenuates vascular injury after ischaemia/reperfusion by inhibiting the Ca2+/calmodulin-dependent protein kinase II pathway. Br J Pharmacol. 2015;172:5619–33.
10. Bailey SM, Udoh US, Young ME. Circadian regulation of metabolism. J Endocrinol. 2014;222:R75–R96.
11. Takeda N, Maemura K. The role of clock genes and circadian rhythm in the development of cardiovascular diseases. Cell Mol Life Sci. 2015;72:3225–34.
12. Troupes CD, Wallner M, Borghetti G, Zhang C, Mohsin S, von Lewinski D, et al. Role of STIM1 (stromal interaction molecule 1) in hypertrophy-related contractile dysfunction. Circ Res. 2017;121:125–36.
13. Chen J, Sysol JR, Singla S, Zhao S, Yamamura A, Valdez-Jasso D, et al. Nicotinamide phosphoribosyltransferase promotes pulmonary vascular remodeling and is a therapeutic target in pulmonary arterial hypertension. Circulation. 2017;135:1532–46.
14. He X, Song S, Ayon RJ, Balisterieri A, Black SM, Makino A, et al. Hypoxia selectively upregulates cation channels and increases cytosolic [Ca^{2+}] in pulmonary, but not coronary, arterial smooth muscle cells. Am J Physiol Cell Physiol. 2018;314:C504–C517.
15. Luo X, Hojayev B, Jiang N, Wang ZV, Tandan S, Rakalin A, et al. STIM1-dependent store-operated Ca^{2+} entry is required for pathological cardiac hypertrophy. J Mol Cell Cardiol. 2012;52:136–47.
16. Hulot JS, Fauconnier J, Ramanujam D, Chaanine A, Aubart F, Sassi Y, et al. Critical role for stromal interaction molecule 1 in cardiac hypertrophy. Circulation. 2011;124:796–805.
17. Correll RN, Goonasekera SA, van Berlo JH, Burr AR, Accornero F, Zhang H, et al. STIM1 elevation in the heart results in aberrant Ca^{2+} handling and cardiomyopathy. J Mol Cell Cardiol. 2015;87:38–47.
18. Xu M, Xue RQ, Lu Y, Yong SY, Wu Q, Cui YL, et al. Choline ameliorates cardiac hypertrophy by regulating metabolic remodelling and UPRmt through SIRT3-AMPK pathway. Cardiovasc Res. 2019;115:530–45.
19. Xue RQ, Yu XJ, Zhao M, Xu M, Wu Q, Cui YL, et al. Pyridostigmine alleviates cardiac dysfunction via improving mitochondrial cristae shape in a mouse model of metabolic syndrome. Free Radic Biol Med. 2019;134:119–32.
20. Xue RQ, Zhao M, Wu Q, Yang S, Cui YL, Yu XJ, et al. Regulation of mitochondrial cristae remodelling by acetylcholine alleviates palmitate-induced cardiomyocyte hypertrophy. Free Radic Biol Med. 2019;145:103–17.
21. Guo L, Yin A, Zhang Q, Zhong T, O'Rourke ST, Sun C. Angiotensin-(1-7) attenuates angiotensin II-induced cardiac hypertrophy via a Sirt3-dependent mechanism. Am J Physiol Heart Circ Physiol. 2017;312:H980–H991.
22. Chen D, Li Z, Bao P, Chen M, Zhang M, Yan F, et al. Nrf2 deficiency aggravates Angiotensin II-induced cardiac injury by increasing hypertrophy and enhancing IL-6/STAT3-dependent inflammation. Biochim Biophys Acta Mol Basis Dis. 2019;1865:1253–64.
23. Vigneault P, Naud P, Qi X, Xiao J, Villeneuve L, Davis DR, et al. Calcium-dependent potassium channels control proliferation of cardiac progenitor cells and bone marrow-derived mesenchymal stem cells. J Physiol. 2018;596:2359–79.

24. Hong Y, Hui SS, Chan BT, Hou J. Effect of berberine on catecholamine levels in rats with experimental cardiac hypertrophy. Life Sci. 2003;72:2499–507.
25. Adameova A, Abdellatif Y, Dhalla NS. Role of the excessive amounts of circulating catecholamines and glucocorticoids in stress-induced heart disease. Can J Physiol Pharmacol. 2009;87:493–514.
26. Liu JJ, Huang N, Lu Y, Zhao M, Yu XJ, Yang Y, et al. Improving vagal activity ameliorates cardiac fibrosis induced by angiotensin II: in vivo and in vitro. Sci Rep. 2015;5:17108.
27. Li M, Zheng C, Kawada T, Inagaki M, Uemura K, Sugimachi M. Adding the acetylcholinesterase inhibitor, donepezil, to losartan treatment markedly improves long-term survival in rats with chronic heart failure. Eur J Heart Fail. 2014;16:1056–65.
28. Suga H. Ventricular energetics. Physiol Rev. 1990;70:247–77.
29. Takeda N, Maemura K. Circadian clock and the onset of cardiovascular events. Hypertens Res. 2016;39:383–90.
30. Thosar SS, Butler MP, Shea SA. Role of the circadian system in cardiovascular disease. J Clin Investig. 2018;128:2157–67.
31. Morris CJ, Purvis TE, Hu K, Scheer FA. Circadian misalignment increases cardiovascular disease risk factors in humans. Proc Natl Acad Sci USA. 2016;113:E1402–E1411.
32. Malliani A, Pagani M, Lombardi F, Cerutti S. Cardiovascular neural regulation explored in the frequency domain. Circulation. 1991;84:482–92.
33. Billman GE. The LF/HF ratio does not accurately measure cardiac sympatho-vagal balance. Front Physiol. 2013;4:26.
34. Young ME, Wilson CR, Razeghi P, Guthrie PH, Taegtmeyer H. Alterations of the circadian clock in the heart by streptozotocin-induced diabetes. J Mol Cell Cardiol. 2002;34:223–31.
35. Hirai T, Tanaka K, Togari A. β-adrenergic receptor signaling regulates Ptgs2 by driving circadian gene expression in osteoblasts. J Cell Sci. 2014;127:3711–9.
36. Lefta M, Campbell KS, Feng HZ, Jin JP, Esser KA. Development of dilated cardiomyopathy in Bmal1-deficient mice. Am J Physiol Heart Circ Physiol. 2012;303:H475–H485.
37. Young ME, Brewer RA, Peliciari-Garcia RA, Collins HE, He L, Birky TL, et al. Cardiomyocyte-specific BMAL1 plays critical roles in metabolism, signaling, and maintenance of contractile function of the heart. J Biol Rhythms. 2014;29:257–76.
38. Alibhai FJ, LaMarre J, Reitz CJ, Tsimakouridze EV, Kroetsch JT, Bolz SS, et al. Disrupting the key circadian regulator CLOCK leads to age-dependent cardiovascular disease. J Mol Cell Cardiol. 2017;105:24–37.
39. Gorski PA, Ceholski DK, Hajjar RJ. Altered myocardial calcium cycling and energetics in heart failure-a rational approach for disease treatment. Cell Metab. 2015;21:183–94.
40. Zhao G, Li T, Brochet DX, Rosenberg PB, Lederer WJ. STIM1 enhances SR Ca^{2+} content through binding phospholamban in rat ventricular myocytes. Proc Natl Acad Sci USA. 2015;112:E4792–E4801.
41. Makarewich CA, Zhang H, Davis J, Correll RN, Trappanese DM, Hoffman NE, et al. Transient receptor potential channels contribute to pathological structural and functional remodeling after myocardial infarction. Circ Res. 2014;115:567–80.
42. Kuwahara K, Wang Y, McAnally J, Richardson JA, Bassel-Duby R, Hill JA, et al. TRPC6 fulfills a calcineurin signaling circuit during pathologic cardiac remodeling. J Clin Investig. 2006;116:3114–26.
43. Kinoshita H, Kuwahara K, Nishida M, Jian Z, Rong X, Kiyonaka S, et al. Inhibition of TRPC6 channel activity contributes to the antihypertrophic effects of natriuretic peptides-guanylyl cyclase-A signaling in the heart. Circ Res. 2010;106:1849–60.
44. Liu QH, Qiao X, Zhang LJ, Wang J, Zhang L, Zhai XW, et al. IK1 channel agonist zacopride alleviates cardiac hypertrophy and failure via alterations in calcium dyshomeostasis and electrical remodeling in rats. Front Pharmacol. 2019;10:929.
45. Rouhana S, Farah C, Roy J, Finan A, Rodrigues de Araujo G, Bideaux P, et al. Early calcium handling imbalance in pressure overload-induced heart failure with nearly normal left ventricular ejection fraction. Biochim Biophys Acta Mol Basis Dis. 2019;1865:230–42.